Journal of Catalysis 271 (2010) 195–200

Contents lists available at ScienceDirect

Journal of Catalysis

journal homepage: www.elsevier.com/locate/jcat

Direct oxidation of methane to methanol over proton conductor/metal mixed catalysts

Byungik Lee [a], Yosuke Sakamoto [b], Daisuke Hirabayashi [b], Kenzi Suzuki [b], Takashi Hibino [a,*]

[a] Graduate School of Environmental Studies, Nagoya University, Furo-cho, Chikusa-ku, Nagoya 464-8601, Japan
[b] Ecotopia Science Institute, Nagoya University, Furo-cho, Chikusa-ku, Nagoya 464-8603, Japan

ARTICLE INFO

Article history:
Received 1 October 2009
Revised 7 January 2010
Accepted 10 January 2010
Available online 4 February 2010

Keywords:
Methane oxidation
Methanol synthesis
Proton conductors
Electrocatalyst

ABSTRACT

The intermediate-temperature and low-pressure production of methanol from methane in a one-pass process was investigated using a micro- or nanosized electrocatalyst system. The powdered catalyst was prepared by mixing proton-conducting $Sn_{0.9}In_{0.1}P_2O_7$ particles with high-activity Pd–Au–Cu/C particles to provide numerous electrolyte–electrode interfaces as reaction sites for methane oxidation. For a feed mixture of H_2O, O_2, and methane, a local electrochemical cell can be formed at the electrode–electrolyte interface: $H_2O \rightarrow 1/2O_2 + 2H^+ + 2e^-$ at the anode site; $O_2 + CH_4 + 2H^+ + 2e^- \rightarrow CH_3OH + H_2O$ at the cathode site. In addition, the electrode also functions as a lead wire that short-circuits the cell. Therefore, the overall reaction can be expected to be $CH_4 + 1/2O_2 \rightarrow CH_3OH$. The series of reactions successfully resulted in reduction in the temperature for initiation of methane oxidation to 250 °C and increased the methanol yield while maintaining a very high selectivity toward methanol for temperatures up to 400 °C.

1. Introduction

Methanol is conventionally produced from methane via high-temperature steam reforming of methane and subsequent high-pressure reaction between H_2 and CO. However, the development of methods for direct oxidation of methane to methanol is desirable, because this is more economic and efficient than the conventional process [1]. While there have been considerable attempts to oxidize methane to methanol in a one-pass process over solid catalysts [2–6], this process has not yet been realized in practical applications, because (a) methane is a very inert reactant, requiring high reaction temperatures (in many cases, $T > 400$ °C) and (b) methanol is an intermediate product, making it difficult to achieve high selectivity at high methane conversion. Other studies have reported the direct oxidation of methane to methanol at lower temperatures ($T > 300$ °C) using oxidants stronger than molecular oxygen, such as N_2O [7,8] and H_2O_2 [9]; however, such oxidants lead to high materials cost.

An alternative approach to the direct oxidation of methane to methanol is to apply an electrochemical cell to the reaction system. We recently reported that methane could be converted into methanol using a solid acid fuel cell capable of operation above 100 °C (Scheme 1a) [10]. Oxidation was performed by the active oxygen species generated at the cathode

$$\text{Anode}: H_2 \rightarrow 2H^+ + 2e^- \quad (1)$$

$$\text{Cathode}: O_2 + 2H^+ + 2e^- \rightarrow (H_2O_2) \rightarrow O^* + H_2O \quad (2)$$

$$CH_4 + O^* \rightarrow CH_3OH \quad (3)$$

The production of methanol and CO_2 over a Pd/C cathode was significant. Furthermore, the addition of Au to Pd increased the methanol formation rate and decreased that of CO_2, the largest effect of which was achieved at a Pd:Au weight ratio of 8:1. These observations are thought to reflect the efficiency of the cathode material for reaction (2) [11,12]. (A similar concept was reported in US Patent No. 5,051,156 [13], although methane activation was conducted at the anode.) However, this approach has two disadvantages over the other approaches already described: (a) the fuel cell-type reactor requires H_2 fuel for the generation of electrical power as well as methanol and (b) the reaction area of the electrochemical cell is inherently lower than that of a solid catalyst.

One approach to overcome these disadvantages is to operate an electrochemical cell without using H_2 fuel and to downsize the cell from macro- to micro- or nanoscale. This may be realized by using H_2O vapor as a proton source for the electrochemical cell.

$$\text{Anode}: H_2O \rightarrow 1/2O_2 + 2H^+ + 2e^- \quad (4)$$

In addition, downsizing may be accomplished by the mixing of electrocatalyst and electrolyte particles, which would provide numerous electrochemical cells in powdered form. In a feed mixture of H_2O, O_2, and methane, H_2O dissociates to protons, electrons, and O_2 at an anodic site of the Pd–Au catalyst, causing a negative

* Corresponding author. Fax: +81 52 789 4894.
E-mail address: hibino@urban.env.nagoya-u.ac.jp (T. Hibino).

0021-9517/$ - see front matter © 2010 Elsevier Inc. All rights reserved.
doi:10.1016/j.jcat.2010.01.011

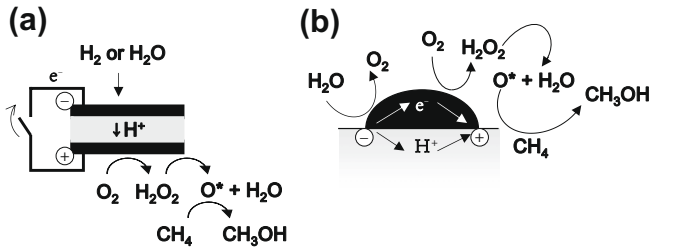

Scheme 1. Schematic illustrations of (a) macro-sized and (b) micro- or nanosized electrochemical cells.

potential. On the other hand, O_2 reacts with protons and electrons to form active oxygen and H_2O, followed by the oxidation of methane to methanol at a cathodic site of the Pd–Au catalyst, causing a positive potential. As a result, a local galvanic cell can be formed at the electrode–electrolyte interface, where reactions (2)–(4) proceed spontaneously, due to self-discharge (Scheme 1b). The following total reaction can be expected:

$$\text{Total reaction}: CH_4 + 1/2O_2 \rightarrow CH_3OH \quad (5)$$

The goals of the present work are to (1) effectively enhance reaction (3) by the addition of a promising promoter (CuO) to the Pd–Au catalyst; (2) evaluate the possibility of using H_2O vapor in place of H_2; and (3) demonstrate the advantage of using local electrochemical cells for the direct synthesis of methanol from methane.

2. Experimental

2.1. Materials

$Sn_{0.9}In_{0.1}P_2O_7$ was prepared as follows: SnO_2 and In_2O_3 were mixed with 85% H_3PO_4 and de-ionized water. The amount of H_3PO_4 used was 1.3 times higher than the stoichiometric value for the preparation of $Sn_{0.9}In_{0.1}P_2O_7$, due to the vaporization of a part of H_3PO_4 during the subsequent heat treatments. The mixture was held stirring at 300 °C until the mixture formed a high viscosity paste. The paste was calcined in a covered alumina crucible at 650 °C for 2.5 h and then ground with a mortar and pestle. The characterization of $Sn_{0.9}In_{0.1}P_2O_7$, including the crystalline structure and composition, has been presented elsewhere [14]. The CuO-impregnated Pd–Au/C (Pd–Au–Cu/C) electrode was prepared as follows. First, CuO was grown on a carbon support (acetylene black) using a co-precipitation method. $[Cu(NH_3)_4](NO_3)_2$ was stirred with carbon in a ethanol/water solution at room temperature. HCl solution was then added dropwise to the suspension until a final pH value of 2.5 was obtained. After filtering, washing, and grinding, the powders were heated in an Ar flow at 450 °C for 2 h. Subsequently, Pd and Au were deposited by an impregnation method. The CuO/C powder was suspended in an ethanol/water solution, and $PdCl_2$ and $HAuCl_4{\cdot}4H_2O$ were added while stirring at approximately 60 °C until the solvent was completely evaporated. Finally, the powder was treated in a 10 vol.% H_2 (Ar balance) feed at 500 °C for 1 h.

2.2. Characterization

The catalysts were characterized using transmission electron microscopy (TEM), energy dispersive X-ray (EDX) spectroscopy, X-ray diffraction (XRD), and X-ray photoelectron spectroscopy (XPS). Specimens for TEM and EDX measurements were prepared by ultrasonic dispersion in *n*-butanol, and a drop of the resultant suspension was evaporated on a Mo grid. Bright-field transmission images and EDX spectra were obtained using a JEOL JEM2100F and JED-2300T, respectively, at an accelerating voltage of 200 kV with a beam current of 92 μA. The XRD patterns were recorded using a Rigaku Miniflex II diffractometer with Cu Kα radiation (λ = 1.5432 Å) as the X-ray source. The diffractometer was operated at 45 kV and 20 mA. The powder diffraction patterns were recorded in the 2θ range from 20° to 80°. The XPS analysis of Cu was conducted using a VG Escallab220i-XL with an Al Kα (1486.6 eV) X-ray source. Photoemission angle was set at 90° to the sample surface, allowing for a reduction in the escape depth to a few nm.

2.3. Electrochemical studies

The $Sn_{0.9}In_{0.1}P_2O_7$ powder was pressed into pellets (Ø12 × 1 mm) under a pressure of 2×10^3 kg cm^{-2}. Two Pt–Au–Cu/C electrodes (0.5 cm^2) were arranged on opposite faces of the electrolyte pellet. A Au reference electrode was attached to the electrolyte surface on the side of the pellet. Two gas chambers were prepared by placing the cell assembly between two alumina tubes. Unless otherwise stated, the anode and cathode chambers were supplied with pure H_2 or 1 vol.% H_2O (Ar balance) and a mixture of 1 vol.% O_2 and 10 vol.% methane (Ar balance), respectively, at a flow rate of 30 mL min^{-1}. Constant currents were applied to the cell using a Hokuto Denko HA-501 galvanostat. The potential of the working

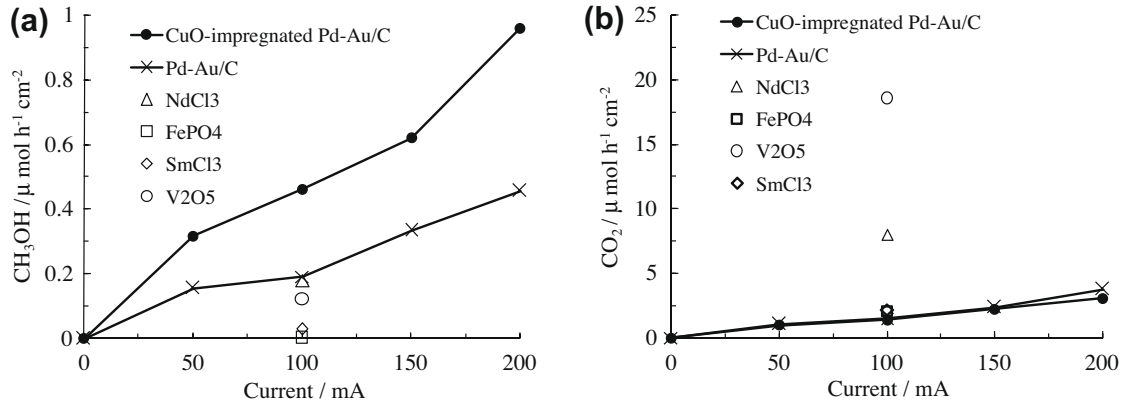

Fig. 1. Electrocatalytic activity of the Pd–Au–Cu/C and Pd–Au/C electrodes (Pd:Au weight ratio = 8:1, Pd + Au = 5 wt.%, Pd–Au–Cu/C loading = 10 mg, electrode area = 0.5 cm^2). Formation rates of (a) methanol and (b) CO_2 as a function of current density at 150 °C. Pure H_2 and a mixture of 1 vol.% O_2 and 10 vol.% methane (Ar balance) were supplied to the anode and cathode, respectively, at a flow rate of 30 mL min^{-1}.

versus the reference electrode was recorded with a Hokuto Denko HE-101 electrometer.

2.4. Catalytic studies

$Sn_{0.9}In_{0.1}P_2O_7$ powder (95 mg) was mixed with Pd–Au–Cu/C powder (5 mg) in a mortar and pestle for a few minutes. Catalytic tests were conducted in a fixed-bed flow reactor. Unless otherwise stated, a mixture of 1 vol.% H_2O, 1 vol.% O_2, and 10 vol.% methane in Ar was fed into the reactor at a flow rate of 30 mL min^{-1}, where the space velocity was 9500 h^{-1}. The outlet gas from the catalyst reactor was analyzed using two online gas chromatographs with flame-ionization (Shimadzu, GC-2014) and thermal-conductivity detectors (Varian CP-4900). The entire gas line was heated at approximately 80 °C, and the gas concentrations were obtained after steady state was attained. The turnover frequencies (TOF) of the catalyst, expressed as mol methanol produced per mol Pd per second, were also estimated, where the number of reaction sites on the Pd surface was measured by the CO pulse method at room temperature. In this case, linear-bonded CO adsorption is assumed to occur on the Pd surface.

3. Results and discussion

3.1. Improvement of Pd–Au catalyst

The addition of a redox metal to the Pd–Au catalyst is considered to be useful to incorporate reaction (3) into the cathode reaction. In preliminary experiments, various metal oxides, chlorides, and phosphates (CuO, V_2O_5, $NdCl_3$, $SmCl_3$, $CuPO_4$, $FePO_4$) were impregnated into Pd–Au/C powder, and their effect on methanol formation were compared using the electrochemical cell. Consequently, CuO was found to exhibit the most significant enhancement among the tested samples, and 1 wt.% CuO was determined to be the optimal value for methanol formation. Fig. 1 shows the methanol and CO_2 formation rates over the Pd–Au–Cu/C cathode at 150 °C, compared with that for the untreated Pd–Au/C cathode. The presence of Cu enhanced the methanol formation while CO_2 formation was kept low. An additional important characteristic of the Pd–Au–Cu/C electrode is the generation of a higher electromotive force (EMF) of 930 mV at 150 °C, compared to the 790 mV for the Pd–Au/C electrode under the same conditions. This may reflect a difference in the cathode reaction path between the two electrodes, as will be discussed later.

The electrode sample was characterized using TEM, XRD, and XPS measurements to determine the Cu environment on Pd–Au/C. The TEM image in Fig. 2a shows spherical-shaped crystals with diameters from several nm to 20–30 nm grown on the carbon surface. EDX analysis (results not shown) of various locations in the TEM image confirmed that the compositions of the crystals were almost pure Pd and Cu, and multi-component Pd–Au and Pd–Au–Cu alloys, independent of the particle size. In some crystals, the Pd or Cu content was distinctly higher than other metal contents, which corresponds to the crystal phase assignments from the XRD measurements (Fig. 2b). However, in other crystals, the EDX intensity was in the order of Pd > Au (very low amounts of Cu were detected.) or Pd > Au > Cu. The Cu 2p XPS spectrum in Fig. 2c has a broad satellite peak (937–947 eV), which provides evidence for the presence of Cu^{2+} ions in the sample [15]. Moreover, the appearance of two separated Cu $2p_{3/2}$ peaks is indicative of the presence of Cu^+ (or Cu^0) in addition to Cu^{2+} ions. The concentration ratio of $Cu^{2+}/(Cu^{2+} + Cu^+$ (or Cu^0)) was estimated to be 0.6 from the relative peak areas for Cu $2p_{3/2}$.

The Cu^{2+}/Cu^+ redox pair assists in the catalysis of both HO· generation from H_2O_2 and the reaction of hydrocarbons with OH·, according to the Fenton mechanism [16,17]:

$$H_2O_2 + H^+ + Cu^+ \rightarrow HO^{\cdot} + H_2O + Cu^{2+} \quad (6)$$

$$R - H + HO^{\cdot} + Cu^{2+} \rightarrow R - OH + H^+ + Cu^+ \quad (7)$$

The cathode potential observed in the measurements of Fig. 1 is in the range of 0.1–0.9 V (versus normal hydrogen electrode (NHE)), which crosses the standard electrode potential of 0.153 V (versus NHE) for Cu^{2+}/Cu^+. Therefore, there is the possibility that the reduction in Cu^{2+} to Cu^+ is promoted by cathodic polarization, allowing for a frequent Cu^{2+}/Cu^+ redox cycle in association with OH· formation and methane oxidation.

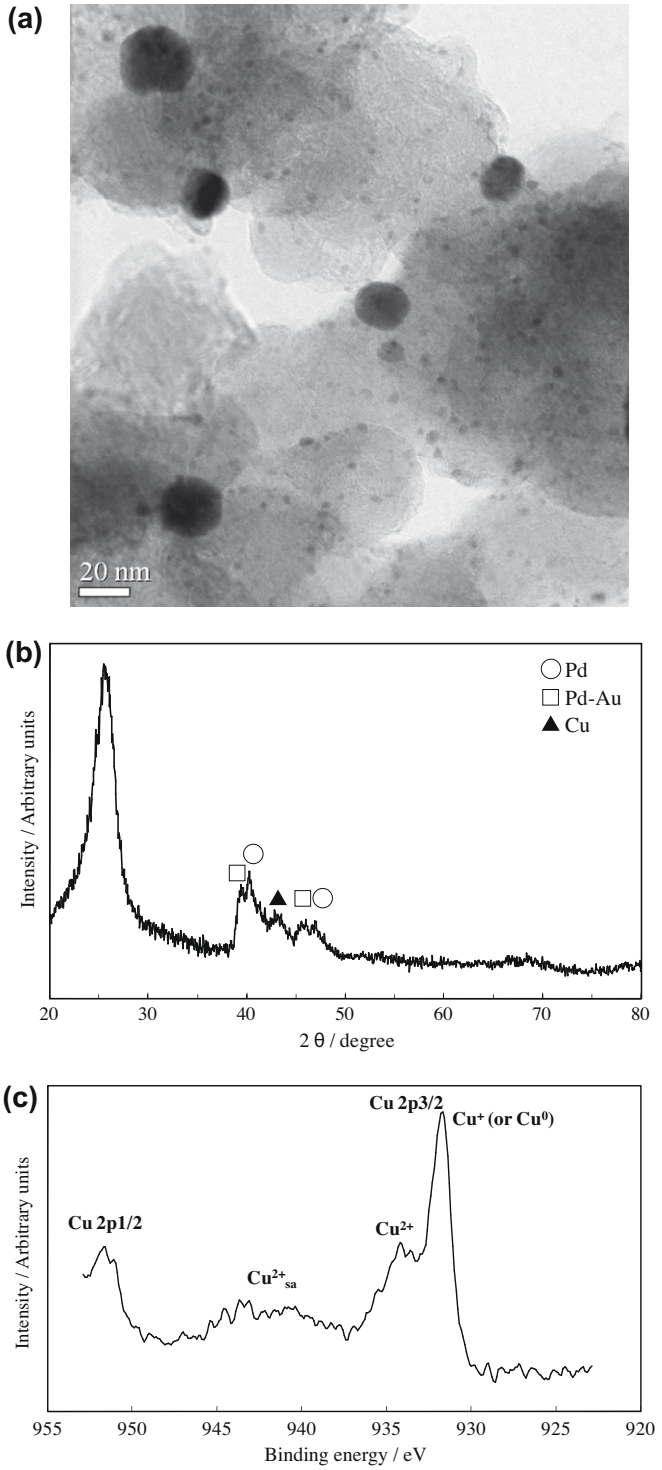

Fig. 2. (a) TEM image, (b) XRD pattern, and (c) XPS spectrum of the Pd–Au–Cu/C electrode.

3.2. Use of H_2O vapor as a proton source for the electrochemical cell

H_2 was used as a fuel in the electrochemical cell for the results given in Fig. 1. H_2O vapor was then employed in place of H_2 to clarify whether the cell could generate electrical power. Fig. 3a displays the temperature dependency of the EMF and the short-circuit current for the cell supplied with 1 vol.% H_2O (Ar balance) into the anode. The EMF and short-circuit current of the cell changed with temperature. The EMF was maintained at approximately 250 mV between 150 and 250 °C, above which it decreased with temperature. The short-circuit current increased with temperature, reached a maximum of 2.5 mA at 350 °C, and then decreased with temperature. Although these performance characteristics are much poorer than those observed with H_2 as the fuel, they fully demonstrate that H_2O can be oxidized to protons and electrons at the anode. The decrease in EMF and short-circuit current observed at elevated temperatures will be explained later.

Fig. 3a also provides other important information about the cathode reaction. The EMF value observed at 150 °C is approximately 4 times higher than an EMF value of 55 mV expected from the Nernst equation for a hydrogen concentration cell

$$E = (RT/2F)\ln[PH_{2anode}/PH_{2cathode}] \quad (8)$$

where PH_{2anode} and $PH_{2cathode}$ can be estimated by assuming that the following equilibrium holds at each electrode

$$H_2 + 1/2O_2 = H_2O \quad (9)$$

(The equilibrium constant, K_{eq}, is 3.2×10^{27} at 150 °C. Both PH_2O_{anode} and $PO_{2cathode}$ were 0.01 atm. PO_{2anode} and $PH_2O_{cathode}$ were previously measured using a Scandia-stabilized zirconia O_2 sensor and dew-point hygrometer, respectively. Therefore, PH_{2anode} and $PH_{2cathode}$ were estimated to be 1.4×10^{-28} and 9.4×10^{-30} atm, respectively.) The discrepancy between the estimated and observed EMF values indicates that the electrode kinetics, especially at the cathode, are determined not only by the partial pressures of H_2O and O_2, but also by those of the other gases, which suggests the contribution of methane to the cathode reaction via reactions (6) and (7). This can also explain the increased EMF in the H_2 fuel cell with the Pd–Au–Cu/C cathode.

Therefore, if the Pd–Au–Cu/C electrode is supplied with a mixture of H_2O, O_2, and methane, a potential difference between the anodic and cathodic sites in the electrode would arise, even if the two sites are exposed to the same gas. (This is due to $Rate_{Eq.\ (4)} \gg Rate_{Eq.\ (2)}$ at the anode and to the opposite relationship at the cathode. As a consequence, each potential was determined by the reaction rate rather than the gas composition.) The electrode also functions as a lead wire; therefore, the cell would be short-circuited. These series of phenomena have been also reported in various gas mixtures, which have been interpreted as a mixed potential at the electrode [18,19]. Methanol was produced under open-circuit conditions at 300 °C or higher, although the methanol yield was only 0.0005% at 300 °C, as shown in Fig. 3b. The temperature dependence of the methanol yield (Fig. 3b) is similar to that for the short-circuit current (Fig. 3a), which suggests a similarity in the electrode reactions for both cells; reactions (4), (2), (6), and (7). Fig. 3b also shows sudden CO_2 formation above 300 °C, which may be due not only to the oxidation of methanol, but also to oxidation of the carbon support, because CO_2 was produced in both the presence and absence of methane at ⩾400 °C or higher. Such carbon combustion also causes a negative potential at the electrode, which explains the reduction in the EMF and short-circuit current over the similar temperature range (Fig. 3a).

Since a mixture of Pd and Cu is a good solid catalyst for direct oxidation of methane to methanol [20], it is difficult to distinguish the electrochemical and non-electrochemical reactions. Therefore, the mixed potentials were estimated from polarization curves for

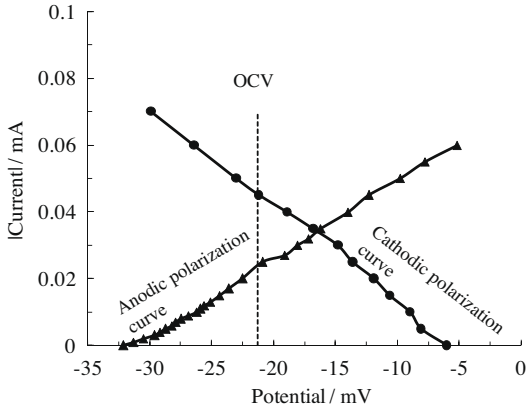

Fig. 4. Comparison of mixed potential and open-circuit potential for the Pd–Au–Cu/C electrode. Anodic polarization curve for 1 vol.% H_2O (Ar balance) and cathodic polarization curve for a mixture of 1 vol.% O_2 and 10 vol.% methane (Ar balance) were measured using the same Pd–Au–Cu/C working electrode at 300 °C. The direction of the cathodic current is reversed. The intersection point of the anodic and cathodic polarization curves corresponds to a mixed potential electrode, where the anodic and cathodic reactions proceed at the same rate. The open-circuit potential were obtained by supplying a mixture of 1 vol.% H_2O, 1 vol.% O_2, and 10 vol.% methane to the Pd–Au–Cu/C working electrode under the same conditions as above.

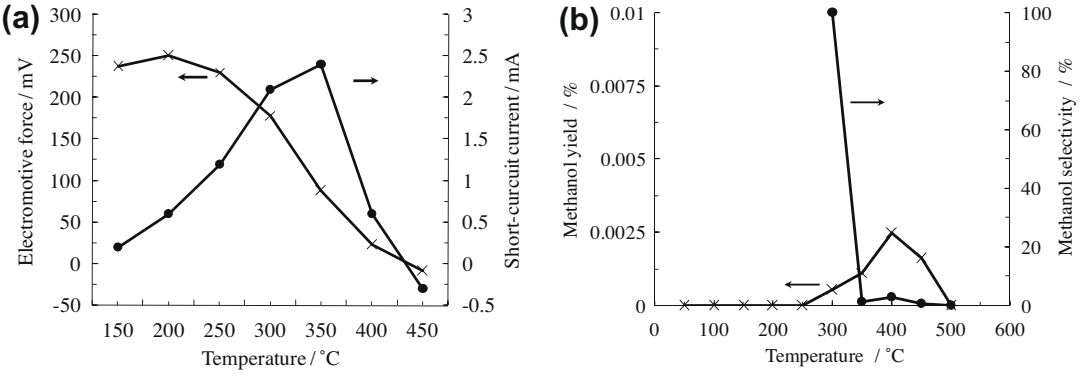

Fig. 3. Electrochemical and electrocatalytic properties of the Pd–Au–Cu/C electrode. (a) EMF and short-circuit current of the electrochemical cell between 150 and 450 °C. H_2O (1 vol.%) (Ar balance) was supplied to the anode, and a mixture of 1 vol.% O_2 and 10 vol.% methane (Ar balance) was supplied to the cathode. The anode always showed negative potential values versus the cathode. (b) Methanol yield and selectivity over the Pd–Au–Cu/C electrode under open-circuit conditions between 50 and 500 °C. A mixture of 1 vol.% H_2O, 1 vol.% O_2, and 10 vol.% methane (Ar balance) was supplied to the electrode.

H_2O oxidation corresponding to reaction (4), and for oxygen reduction and subsequent methane oxidation corresponding to reactions (2), (6), and (7), and these were compared with the open-circuit potentials of the working electrode in the mixture of H_2O, O_2, and methane. As an example, Fig. 4 displays the anodic polarization curves of H_2O and the cathodic polarization curves of a mixture of O_2 and methane at 300 °C. The intersection point of the anodic and cathodic polarization curves, which corresponds to the mixed potential, was approximately in agreement with the open-circuit potential value, which demonstrates that reactions (4), (2), (6), and (5) occur at the electrode under open-circuit conditions. In other words, the small discrepancy between the two potentials may be due to non-electrochemical reaction over the Pd–Au–Cu catalyst.

3.3. Methane oxidation over the $Sn_{0.9}In_{0.1}P_2O_7$ and Pd–Au–Cu/C mixed catalyst

The mixed potential phenomenon enables the elimination of an external power source and circuit from the reaction system. However, the reaction area of the electrochemical cell is not sufficiently high to meet the criteria for practical application. Therefore, the phenomenon was then applied to heterogeneous catalytic systems. The activity of a mixed electrolyte and electrode catalyst for methane oxidation was measured from 50 to 500 °C in a feed mixture of 1 vol.% H_2O, 1 vol.% O_2, and 10 vol.% methane (Ar balance). Fig. 5 shows the methanol yield and selectivity as a function of temperature, in addition to data for the individual materials. CO_2 was produced rather than methanol over the individual materials, Pd–Au–Cu/C and $Sn_{0.9}In_{0.1}P_2O_7$, at temperatures above 350 °C. In contrast, the $Sn_{0.9}In_{0.1}P_2O_7$ + Pd–Au–Cu/C mixed catalyst successfully catalyzed the production of methanol with high selectivity toward methanol at temperatures above 200 °C. (Gas analyses did not indicate significant quantities of products other than methanol and CO_2; therefore, it is likely that methanol reacts with $OH^{\cdot}$ radicals to form CO_2 at a very fast rate over the mixed catalyst.) An important result is that the resultant methanol yield at 400 °C is approximately 3 times larger than that obtained for the electrochemical cell (Fig. 3b), despite the use of a smaller amount of Pd–Au–Cu/C in the former (5 mg) than that in the latter (10 mg). More importantly, the TOF value estimated at 400 °C was 0.032 s^{-1}, which is higher TOF values of 0.003 and 0.008 s^{-1} reported for V_2O_5/SiO_2 at 560 °C and MoO_3/SiO_2 at 590 °C [21], respectively. Thus, it is concluded that the $Sn_{0.9}In_{0.1}P_2O_7$ + Pd–Au–Cu/C mixed catalyst shows a relatively high catalytic activity for the methanol formation at lower temperatures.

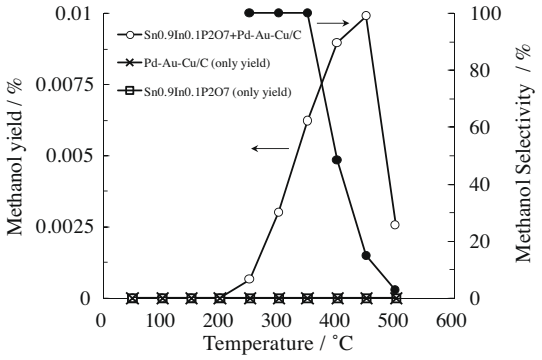

Fig. 5. Catalytic properties of the $Sn_{0.9}In_{0.1}P_2O_7$ + Pd–Au–Cu/C mixed catalyst. Methanol yield and selectivity over the $Sn_{0.9}In_{0.1}P_2O_7$ + Pd–Au–Cu/C mixed catalyst between 50 and 500 °C. The weight percentages of $Sn_{0.9}In_{0.1}P_2O_7$ and Pd–Au–Cu/C in the mixed catalyst were 95 and 5 wt.%, respectively. Methanol yields over individual $Sn_{0.9}In_{0.1}P_2O_7$ and Pd–Au–Cu/C materials with the same electrolyte, metal, or carbon content as $Sn_{0.9}In_{0.1}P_2O_7$ + Pd–Au–Cu/C are included for comparison. A mixture of 1 vol.% H_2O, 1 vol.% O_2, and 10 vol.% methane was supplied to the catalyst.

In order to gain insight into the above results, methanol synthesis was conducted over different mixed catalysts of $Sn_{0.9}In_{0.1}P_2O_7$ + Pd–Au/C and SnP_2O_7 + Pd–Au–Cu/C. Fig. 6a shows that the $Sn_{0.9}In_{0.1}P_2O_7$ + Pd–Au/C mixed catalyst gives a lower methanol yield than the $Sn_{0.9}In_{0.1}P_2O_7$ + Pd–Au–Cu/C mixed catalyst, which is consistent with the results observed for the electrochemical cell (Fig. 1). More importantly, the methanol yield over SnP_2O_7 + Pd–Au–Cu/C was lower than that over $Sn_{0.9}In_{0.1}P_2O_7$ + Pd–Au–Cu/C. Our previous study showed that the proton conductivity of SnP_2O_7 ranged from approximately one-half to one-third that of $Sn_{0.9}In_{0.1}P_2O_7$ [14], which suggests that methane oxidation over the mixed catalyst relies on proton migration through the electrolyte material.

Evidence for the suggested contribution of proton conductivity is provided by the catalytic activity of the $Sn_{0.9}In_{0.1}P_2O_7$ + Pd–Au–Cu/C mixed catalyst under various conditions. Fig. 6b shows that the methanol yield was considerably decreased under dry conditions (PH_2O = ~0.006 atm), due to the decrease in the proton conductivity of $Sn_{0.9}In_{0.1}P_2O_7$ [14]. The H/D isotope effect on the

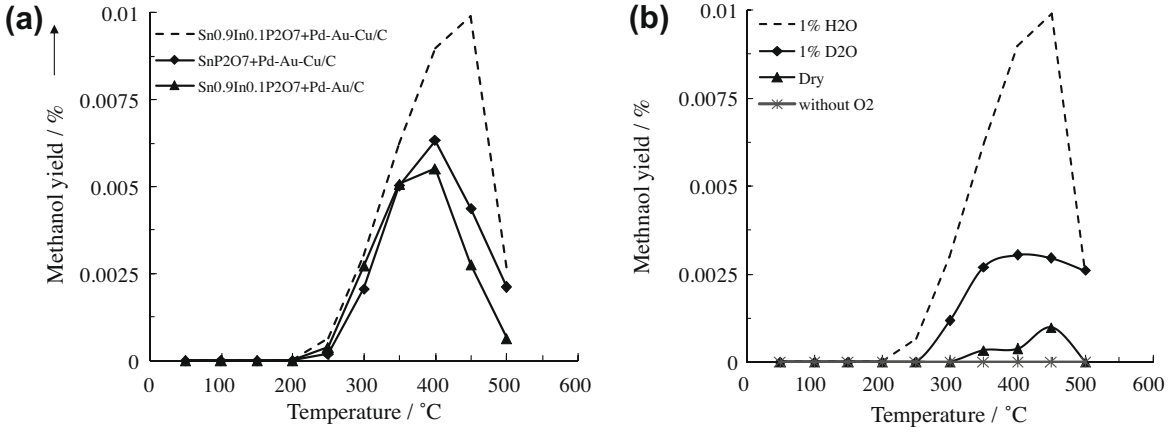

Fig. 6. Catalytic properties of different mixed catalysts under various conditions. (a) Methanol yield over $Sn_{0.9}In_{0.1}P_2O_7$ + Pd–Au/C and SnP_2O_7 + Pd–Au–Cu/C between 50 and 500 °C. A mixture of 1 vol.% H_2O, 1 vol.% O_2, and 10 vol.% methane (Ar balance) was supplied to the catalyst. (b) Methanol yield over the $Sn_{0.9}In_{0.1}P_2O_7$ + Pd–Au–Cu/C mixed catalyst under various conditions. Three mixtures of 1 vol.% O_2 and 10 vol.% methane (Ar balance), 1 vol.% D_2O, 1 vol.% O_2, and 10 vol.% methane (Ar balance), and 1 vol.% H_2O and 10 vol.% methane (Ar balance) were supplied to the catalyst. PH_2O in the first mixture was measured as ~0.006 atm using a dew-point hygrometer.

activity of the mixed catalyst is helpful to further clarify this point, because the electrical resistance of proton conductors is commonly increased by replacing protons with deuterons [21]. The methanol yield was significantly reduced by using D_2O vapor in place of H_2O vapor (Fig. 6b); however, the observed effect was more expected. A possible reason for this is that in addition to proton migration through the $Sn_{0.9}In_{0.1}P_2O_7$ bulk, reaction (4) may also be suppressed by using D_2O vapor. For example, the H/D isotope effect reported for $SrCe_{0.95}Yb_{0.05}O_{3-\alpha}$ was observed not only for proton migration, but also for electrode kinetics related to protons, causing a multiplied effect [22]. Regardless, the presence of H_2O is shown to be a necessary factor for methane oxidation. In addition, it is not surprising that the presence of O_2 is another important factor for methane oxidation (Fig. 6b). These results are interpreted as an indication that methane oxidation proceeds according to Scheme 1b.

The present approach would also be useful for homogeneous catalytic systems. To date, these systems have been used to convert methane to methanol with high selectivity at low temperatures (ca. 100 °C), but require high-pressure conditions (ca. 50 atm) [23]. It is therefore expected that use of the $Sn_{0.9}In_{0.1}P_2O_7$ + Pd–Au–Cu/C mixed catalyst in liquid systems would reduce the required reaction temperature and pressure.

4. Conclusions

A new scheme for direct methane oxidation to methanol was proposed using the $Sn_{0.9}In_{0.1}P_2O_7$ proton conductor and highly active Pd–Au–Cu/Ct. When a mixture of H_2O, O_2, and methane is introduced to the Pt–Au–Cu/C electrode, methane is oxidized to methanol at $\geqslant$300 °C or above. The reaction mechanism was shown to be based on the mixed potential at the electrodes, where H_2O is oxidized at the anode site and methanol is produced via O_2 reduction at the cathode site. This series of reactions is also applicable to the $Sn_{0.9}In_{0.1}P_2O_7$ + Pd–Au–Cu/C mixed catalyst. Methanol synthesis over the mixed catalyst was characterized by two major features; yields that were approximately one order of magnitude higher than that observed for the electrochemical cell and high selectivity in the temperature range of 250–350 °C. However, challenges still remain for further improvement in the performance of such catalysts systems, especially in terms of the methane conversion efficiency. Further research efforts are required to realize the development of ideally active materials for methane oxidation by active oxygen.

References

[1] R. Pitchai, K. Klier, Catal. Rev. Sci. Eng. 28 (1986) 13.
[2] N.D. Spencer, J. Catal. 109 (1988) 187.
[3] Z. Sojka, R.G. Herman, K. Klier, J. Chem. Soc., Chem. Commun. (1991) 185.
[4] A. Parmaliana, F. Frusteri, A. Mezzapica, M.S. Scurrel, N. Giordano, J. Chem. Soc., Chem. Commun. (1993) 751.
[5] T. Kobayashi, K. Nakagawa, K. Tabata, M. Haruta, J. Chem. Soc., Chem. Commun. (1994) 1609.
[6] A. de Lucas, J.L. Valverde, P. Canizares, L. Rodriguez, Appl. Catal. A: Gen. 184 (1999) 143.
[7] J.A. Barbero, M.A. Bañares, M.A. Peña, J.L.G. Fierro, Catal. Today 71 (2001) 11.
[8] M.M. Khan, G.A. Somorjai, J. Catal. 91 (1985) 263.
[9] Y. Wang, K. Otsuka, J. Catal. 155 (1995) 256.
[10] A. Tomita, J. Nakajima, T. Hibino, Angew. Chem. Int. Ed. 47 (2008) 1462.
[11] D.I. Enache, J.K. Edwards, P. Landon, B. Solsona-Espriu, A.F. Carley, A.A. Herzing, M. Watanabe, C.J. Kiely, D.W. Knight, G.J. Hutchings, Science 311 (2006) 362.
[12] T. Ishihara, Y. Ohura, S. Yoshida, Y. Hata, H. Nishiguchi, Y. Takita, Appl. Catal. A 291 (2005) 215.
[13] B. Scharifker, O. Yépez, J.C. De Jesús, M.M. Ramírez de Agudelo, US Patent No. 5,051,156, 1991.
[14] M. Nagao, A. Takeuchi, P. Heo, T. Hibino, M. Sano, A. Tomita, Electrochem. Solid-State Lett. 9 (2006) A105.
[15] M.A. Salim, G.D. Khattak, N. Tabet, L.E. Wenger, J. Electron. Spectrosc. Relat. Phenom. 128 (2003) 75.
[16] D.H. Flint, R.M. Allen, Chem. Rev. 96 (1996) 2315.
[17] K. Otsuka, I. Yamanaka, Catal. Today 57 (2000) 71.
[18] N. Miura, G. Lu, N. Yamazoe, H. Kurosawa, M. Hasei, J. Electrochem. Soc. 143 (1996) L33.
[19] F.H. Garzon, R. Mukundan, E.L. Brosha, Solid State Ionics 136–137 (2000) 633.
[20] M. Lin, T. Hogan, A. Sen, J. Am. Chem. Soc. 119 (1997) 6048.
[21] M. Faraldos, M.A. Bañares, J.A. Anderson, H. Hu, I.E. Wachs, J.L.G. Fierro, J. Catal. 160 (1996) 214.
[22] T. Hibino, K. Mizutani, H. Iwahara, J. Electrochem. Soc. 140 (1993) 2588.
[23] Y. Seki, N. Mizuno, M. Misono, Appl. Catal. A 158 (1997) L47.